Measurement 210 (2023) 112552

Contents lists available at ScienceDirect

Measurement

journal homepage: www.elsevier.com/locate/measurement

Evaluation and metrological performance of a novel ionisation vacuum gauge suitable as reference standard

Karl Jousten [a,*], Sylke Bechstein [a], Matthias Bernien [a], Frédéric Boineau [b], Nenad Bundaleski [c], Claus Illgen [a], Berthold Jenninger [d], Janez Šetina [e], Ricardo A.S. Silva [c], Anke Stöltzel [d], Orlando M.N.D. Teodoro [c], Martin Wüest [f]

[a] Physikalisch-Technische Bundesanstalt (PTB), Abbestr. 2-12, 10587 Berlin, Germany
[b] Laboratoire national de métrologie et d'essais (LNE), 1 rue Gaston Boissier, 75724 Paris Cedex 15, France
[c] CEFITEC, Department of Physics, Faculty of Sciences and Technology, Nova University of Lisbon, 2829-515 Caparica, Portugal
[d] CERN European Organization for Nuclear Research, 1211 Geneva 23, Switzerland
[e] IMT Institute of Metals and Technology, Lepi pot 11, 1000 Ljubljana, Slovenia
[f] INFICON AG, Alte Landstrasse 6, LI-9496 Balzers, Liechtenstein

ARTICLE INFO

Keywords:
Ionisation vacuum gauge
Hot cathode
Sensitivity
Secondary electrons
Ion induced secondary electron yield

ABSTRACT

Recently, a new type of ionization vacuum gauge was introduced, which was proposed as a reference and transfer standard in the range of 10^{-6} Pa to 10^{-2} Pa because of its excellent stability and linearity. In contrast to present models of ionisation vacuum gauges, all electrons have a well-defined path length through the ionisation space. This even allows one to predict the sensitivity for a gas species provided that the ionisation cross section of the gas molecules for electrons between 50 eV and 200 eV is known. Following the development of this gauge we investigated its metrological performance in terms of linearity, resolution, repeatability, reproducibility, transport and long-term stability, disturbances by magnetic fields, influence of the surrounding earth potential and so on. The gauge demonstrated excellent metrological properties and is indeed suitable as an accurate reference and transfer standard, but can also provide important economic benefits to manufacturers and users.

1. Introduction

In a recent review [1] it was concluded that the Bayard-Alpert design of an ionisation vacuum gauge does not offer the potential of a vacuum gauge with satisfying stability for metrological needs. Instead, the authors proposed a design similar to the idea of Klopfer [2]. This new design was developed by Jenninger et al. [3] and first experimental metrological results were published in [4].

In this paper we report on comprehensive experimental work on the metrological performance of the new gauge design. Experiments are complemented by simulations of the electron and ion trajectories inside of the gauge investigating external influences like magnetic fields and minor modifications of the electrode design. The latter investigations are needed to distinguish between mandatory functional elements for the performance of the gauge and possible modifications, because the design is under development as a written Technical Specification (ISO TS 6737) by ISO TC 112. For this reason, we recommend to call this new design of an ionisation vacuum gauge in short "ISO gauge", when the Technical Specification has been published.

In the following section we will shortly summarize the already published design of the ISO gauge. In Section 3 we present investigations on variations of the nominal potentials and electrode dimensions. Section 4 reports on experiments characterizing its metrological performance such as linearity, repeatability and reproducibility of sensitivity, resolution, and robustness. The influence of magnetic fields is described in Section 5. Section 6 deals with experimental results of relative gas sensitivity factors and Section 7 discusses and summarises the metrological performance of the gauge.

2. Design and operation of the novel ionisation vacuum gauge

Fig. 1 shows the design as developed on the basis of simulations [3]. The functional elements are the electron emitting cathode surrounded by a Wehnelt-cylinder [5], the two parts of the anode cage, the ion

* Corresponding author.
E-mail address: karl.jousten@ptb.de (K. Jousten).

https://doi.org/10.1016/j.measurement.2023.112552
Received 16 November 2022; Received in revised form 23 January 2023; Accepted 27 January 2023
Available online 10 February 2023

collector, the electron deflector, and the Faraday cup with the nominal potentials shown in the figure.

The Wehnelt cylinder surrounding the hot thermionic cathode controls and collimates the electron beam into the anode cage. The so formed electron beam (red in Fig. 1) in the left part of the model passes through the anode cage and exits to the right into the Faraday cup. The first quarter of the anode cage ($V_A = 250$ V), the ion collector ring ($V_C = 0$ V) and the second remaining part of the anode cage ($V_A = 250$ V) form an electrostatic lens which focuses the electron beam into the circular exit of the anode cage. Behind the exit the electron beam is deflected by the deflector electrode ($V_D = 45$ V) in a U-turn onto the capturing part of the Faraday cup (V_F: 248 V to 280 V). The effect of the U-turn and the deflector is threefold:

1. It is ensured that the X-rays produced by the electrons hitting the surface have a very low probability to reach the ion collector where they would generate secondary electrons which are indistinguishable from arriving ions.
2. Secondary or reflected primary electrons are repelled onto the Faraday cup.
3. Ions generated behind the anode cage exit or desorbed from the Faraday cup surface are driven to the deflector.

The ions generated by the electron beam inside the anode cage are accelerated towards the ion collector which consists of the mentioned ring and a rod reaching into the larger space of the anode cage. Ions generated behind the exit of the anode cage are mainly accelerated towards the deflector electrode.

The measured ion current is proportional to the gas density inside the volume occupied by the electron beam, the ionisation cross section of the gas molecules by electron impact, the effective path length of the electrons inside the anode cage and the electron current.

Due to the focussing inside the anode cage, the electron current should not exceed 200 μA. Higher currents, depending on the prevailing gas species, can lead to a saturation of ionisation by ionising all molecules within the spatial range of the electron beam and cause non-linearities.

The effective electron path length is accurately defined by the length of the anode cage and to a smaller extent by the potential inside it. Any changes of the emission points of the electrons on the cathode will not significantly change the path length in contrast to existing ionisation gauge types, e.g. of Bayard-Alpert. Also, space charge effects around the ion collector do not alter the electron path length.

Ions desorbed by electron impact in the Faraday cup will reach the deflector but not the ion collector. Electron stimulated desorption of neutrals in the Faraday cup, however, will contribute to the gas density in the gauge and therefore to the ion current.

The stability of sensitivity is greatly improved compared to existing ionisation vacuum gauge types for the following reasons:

- All electrons have nearly the same path length through the volume of ionisation, independent of their origin on the cathode
- Changes of the thermionic emission by temperature or work function changes of the cathode do not affect sensitivity
- Space charge does not affect the electron trajectories significantly
- The anode is not hit by electrons which would generate X-rays and secondary electrons
- Except for the cathode, the design does not require any grid or wire which tend to be unstable, in particular during transports
- A cathode exchange does not alter the sensitivity

Due to the relatively low electron emission current I_e and hence low generated ion current I_C the measurement range is limited to about 10^{-6} Pa at the lower end for drift and noise of the ion current measurement. At the upper end, linearity and accuracy is lost beyond about 10^{-2} Pa due to the relatively high sensitivity of 0.289 Pa^{-1} (nitrogen) and the mean free path of ions and electrons.

Another important benefit of this gauge is that the sensitivity does not depend on the individual gauge. Fig. 4 in [4] shows that the sensitivities for nitrogen of 0.289 Pa^{-1} varied by less than 2.5 % for 12 gauges from two different manufacturers.

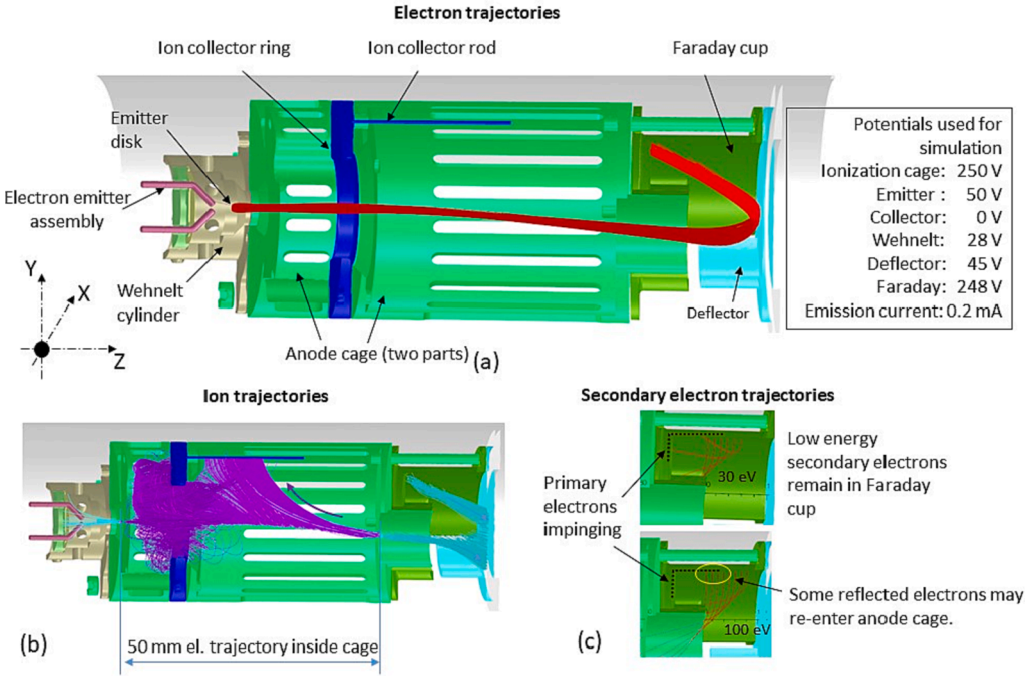

Fig. 1. Design and charged particle trajectories of the novel gauge, from [3]. Top (a): the electrode arrangement and electron trajectories (in red) with the potentials and emission current used for the simulation. Bottom left (b): ion trajectories. The purple trajectories correspond to those that are collected by the ion collector. The light blue ones are those that are rejected. Bottom right (c): Trajectories of secondary electrons leaving the surface perpendicular with the indicated kinetic energy.

3. Optimum potentials and possible variations of electrodes

The potentials listed in Fig. 1 were the design parameters for the simulations. As parameters for optimisation, electron transmission efficiency T_e (apparent current on Faraday I_F/cathode emission current I_e) and ion collection efficiency $c_{ion,C}$ (ions arriving on the collector/total number of generated ions within the ionisation space) were used. The total electron emission current splits into the current I_F arriving on the Faraday cup and a small part I_A arriving on the anode.

$$I_e = I_F + I_A \tag{1}$$

The electron transmission efficiency T_e is defined as

$$T_e = \frac{I_F}{I_e} \tag{2}$$

The relative high electron energy of 200 eV compared to typically 100 eV in Bayard-Alpert gauges was necessary to ensure a narrow electron beam in its full length. Smaller energies would lead to a widening of the beam due to space charge effects.

We mainly used ES-042 Tantalum discs from Kimball Physics Inc. as a cathode and, in a few cases, an yttria-coated iridium disc cathode ES-535 from the same company was used. Both are mounted on an AEI standard ceramic base which is common for electron microscopes. In one case, we replaced the disc emitter by a U-shape tungsten wire, where the top of the "U" was located on the same plane as the emitter disc, and obtained similar performance as with the disc cathodes. We found that a lifetime of more than 10 000 h can be expected for the ES-042 Ta cathode in residual gas and inert gases, when the heating current is kept below 1.6 A.

After experiments it turned out that the potential V_W of the Wehnelt should be optimised in order to increase the current I_F onto the Faraday cup and T_e without changing the sensitivity. For this reason, we recommend a Wehnelt voltage of 34 V instead of the 28 V used for the simulation (see Table 1). A graph of measured electron transmission efficiency T_e (simulated and measured) and measured Faraday current in dependence of the Wehnelt potential is shown in Fig. 3 of [4] for a well aligned cathode disc. Fig. 3 here shows a similar graph for a less well aligned cathode disc. While we observed a flat curve of T_e vs Wehnelt potential until 34 V for a well aligned cathode disc, here we see a pronounced minimum near 25 V. In the figure, we added the result of a simulation by COMSOL, where the centre of the cathode disk was 1 mm off axis and the surface normal put to an angle of 30° with respect to the Wehnelt cylinder axis instead of 0°. Qualitatively, the two curves of simulation and experiment are very similar, which let us conclude that this characteristic is due to some misalignment. The gauge, however, still performed rather well when operating at a Wehnelt potential of 33 V to 34 V.

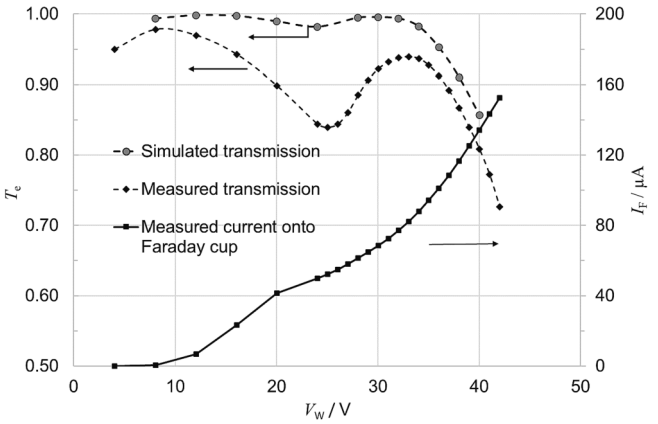

Fig. 3. Electron transmission efficiency T_e (simulated and measured) and measured Faraday current in dependence of the Wehnelt potential for less well aligned cathode.

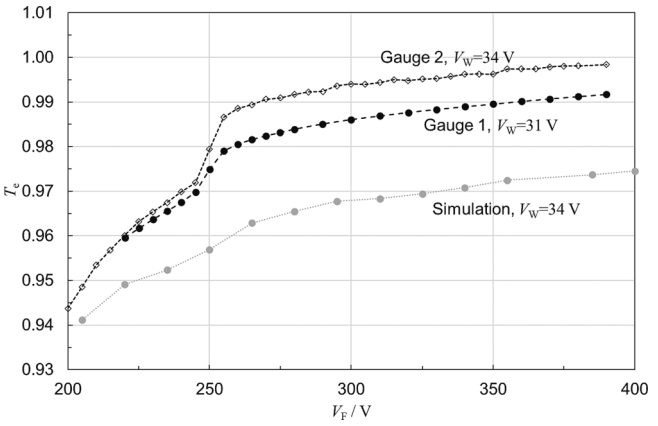

Fig. 4. Electron transmission T_e to the Faraday in dependence of the Faraday potential V_F. for two different gauges and two different Wehnelt potentials V_W.

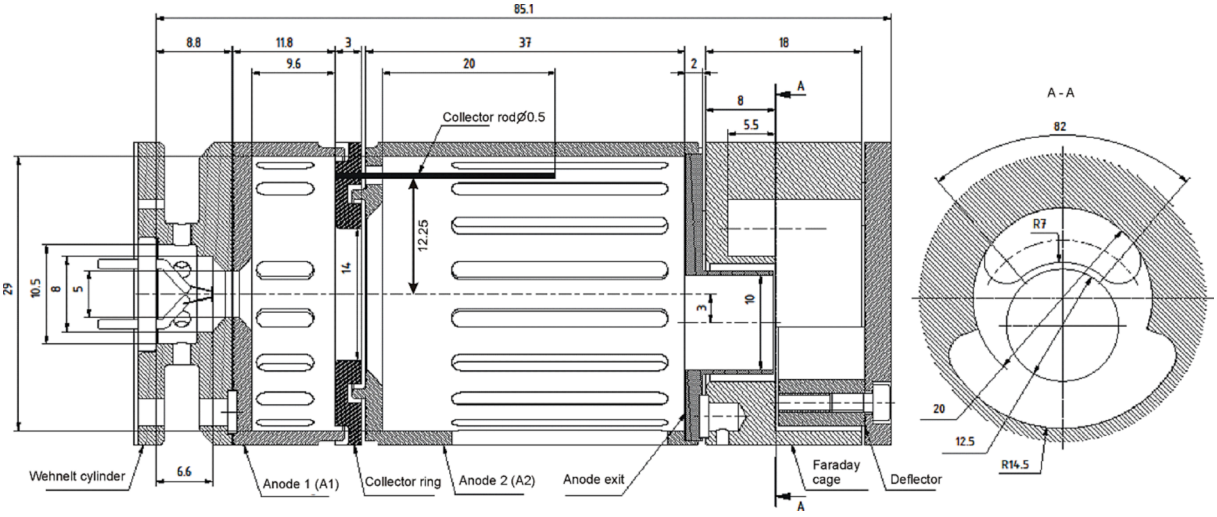

Fig. 2. Example of a drawing realising the recommended dimensions of the novel gauge (by courtesy of VACOM GmbH). 17 slits, 2 mm wide, in the anode cylinder are placed every 20° on the cylinder circumference, but none near the collector rod at 0°.

It was also found that increasing the Faraday cup potential beyond the value of 248 V used in the simulation increases T_e (Fig. 4). In addition, around the Faraday potential of 250 V T_e shows a kind of step, so that for a slightly changing Faraday potential the electron transmission will change by a larger extent than in the flatter part near 280 V, which we recommend when using the gauge (see Table 1). The sensitivity, however, did not change by changing the Faraday potential. The reason for the apparent increase of T_e with Faraday voltage (Fig. 4) is threefold [6]:

- Less secondary electrons escape from the Faraday cup (important in the range 240 V – 260 V)
- Backscattering of electrons is reduced with increasing impact energy
- More backscattered electrons remain in the Faraday cup.

Computer simulations by SIMION showed that electron trajectories inside the anode cage and the circular exit are not affected by the Faraday potential, thus explaining why the sensitivity is invariant to this potential. The simulation, which includes the simulation of the secondary electron emission process from stainless steel [6], however, showed that there is decreasing escape of electrons from the Faraday cup when its potential is increased. Although T_e obtained in the simulations is systematically few percent lower than the experimental values (the source of this systematic discrepancy is discussed in [6]), good agreement between the simulated and experimental curves was obtained (Fig. 4).

While higher voltages than the recommended 280 V lead to even higher T_e, they also lead to a higher risk of leakage currents or even sparkover.

We also varied the potential of the deflector around its nominal value of 45 V and found that (i) the nominal value is optimal in terms of sensitivity and (ii) small variations do not alter the sensitivity significantly. We concluded that a stability of all the voltage sources of ± 0.5 % around the nominal value will be sufficient to have insignificant influence (<0.1 %) on the gauge sensitivity (see Table 1).

While most of the electrode dimensions and distances need to be fixed in order not to change electron and ion trajectories in a significant manner, some modifications may not alter these. To this end, we investigated the necessity of the shield at the bottom of the Wehnelt cylinder, the shape of the Wehnelt near the cathode and the openings of the anode cage by simulations. In the following, we report on the results. It needs to be noted that we did not verify these simulations by experiments, so that we still recommend the design proposed in the previous section in Fig. 2:

- Shield:

The shield at the bottom of the Wehnelt, normally at the same potential, has the function to protect the ceramic disk of the cathode from coating and charging up and to have a well-defined potential around the emitting part of the cathode. We varied the potential of the shield including the normally floating ceramics from 5 V to 200 V, while the Wehnelt was kept at 28 V or 34 V. The sensitivity of the gauge remained constant within ± 0.3 %, statistically not significant, and the electron beam widened only slightly at higher potentials. From the electrostatic point of view, this indicates that the shape of the shield may be modified or even omitted (provided that the emitting part of the cathode sits at the same position within the Wehnelt) without loss of performance of the gauge, but the issue of covering the ceramics remains.

- Simplified Wehnelt structure:

The emitting plane of the cathode disk is positioned at the wider end of the cone part of the Wehnelt. Towards the left (see Fig. 2), it follows a cylindrical part of 1.8 mm length and 8 mm diameter, which then widens stepwise to a cylindrical part of 10.5 mm diameter. Replacing the 8 mm diameter cylindrical part with 10.5 mm, - which simplifies manufacturing, did not alter the sensitivity significantly (within 0.5 %), but widened the electron beam somewhat, which may increase the risk of reducing T_e.

- Openings in anode cage and envelope of the gauge:

The longitudinal openings in the anode cage cylinders ensure the free exchange of gas molecules with the outer volume. On the other hand, the openings must not be too large, so that the penetration of the ground potential into the anode compartment does not become too strong. Between these opposing requirements the manufacturer can decide how to design the openings of the anode cage. We decided to use slotted openings in the anode cylinder with the exception near the collector rod. Near this rod it is very important to have the electric field pointing to the rod from all directions, including from the anode cylinder, in order to maintain the high ion collection efficiency $c_{ion,C}$.

We investigated for our slit design, if T_e or $c_{ion,C}$ significantly depends on the diameter of the envelope DN40 or DN63 (40 mm or 63 mm inner diameter). Although the field penetration was larger for DN40, neither T_e nor $c_{ion,C}$ were significantly affected. This means that the gauge may be mounted either in any of the mentioned tubes tube without significant change of performance.

We also varied the number of slits by omitting the two nearest to the collector rod. Also here, we found no significant change for T_e or $c_{ion,C}$. A clear criterion for the permissible area of an opening could be the subject of future work.

4. Metrological characterization

Some metrological characterization of this gauge was already reported by us in [4]. One of the features is the excellent linearity or constant sensitivity from 10^{-6} Pa to 10^{-2} Pa shown in Fig. 5 in [4]. Another important feature reported in [4] was the low spread of sensitivities (≤ ±1.2 %) between different copies of the gauge, even from different manufacturers (Fig. 4 in [4]). In particular this feature has potential economic benefits for manufacturers and users of the gauge: If a measurement uncertainty of 5 % is sufficient, manufacturers do not need to calibrate the gauge after production and users have no need for recalibrations, e.g. after cathode replacement, and can exchange the gauge without any process adjustment.

All following measurements were carried out with gauges manufactured by two different companies according to the design shown in Fig. 1 and Fig. 2. Slight modifications were made, not relevant for

Table 1
Comparison of potentials used for optimum performance in simulation and recommended values for optimum experimental performance. Tolerance for all potentials: ±0.5 %.

Electrode	Symbol	Simulation	Experimental optimum	Note
Cathode (emitter)	V_C	50 V	50 V	
Wehnelt	V_W	28 V	34 V	34 V less sensitive to misalignment of cathode and higher emission current
Anode	V_A	250 V	250 V	
Deflector	V_D	45 V	45 V	Flat maximum around this voltage for sensitivity and electron transmission
Faraday	V_F	248 V	280 V	280 V leads to higher electron transmission

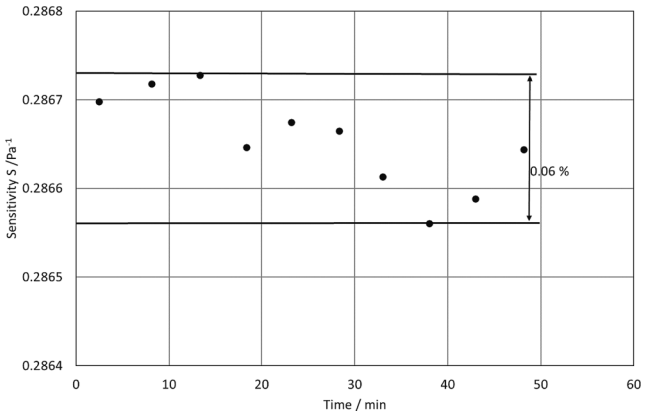

Fig. 5. Sensitivity after 10 consecutive repeated pressure generations at 1×10^{-5} Pa within 50 min.

electron and ion trajectories.

For the highest accuracy, we applied the following conditioning procedure of the gauge: After a bake-out (150 °C for at least 48 h) the gauge was operated in Ar at 5 mPa. It was found that under bombardment of Ar ions a hydrocarbon layer is grown by polymerization of hydrocarbons on the surface of the collector [7]. A sufficiently thick hydrocarbon layer stabilizes the ion induced secondary electron yield (IISEY) on the collector and thus the sensitivity [7]. The necessary time of Ar bombardment for a sufficient stability of IISEY will depend on the partial pressure of hydrocarbons in the vacuum system, but also on the type of ions as can be seen from Table 2. Clearly, the effect of the hydrocarbon layer is higher for helium ions than for the heavier nitrogen and argon ions. While for the measurement of Ar a conditioning time of 1 h was sufficient, for N_2 2 h and for He a time of at least 6 h seem necessary to stabilise the yield to within 1 %. For highest accuracy, we recommend a conditioning time of 3 h (electron emission current 30 μA), respectively 5 h when a light gas like helium be measured.

To estimate the size of the thermal transpiration effect inside the gauge, we measured the electrode temperatures with the cathode heated. Clearly, the Wehnelt cylinder with 120 °C is the hottest electrode except of the cathode, while anode and collector have temperatures between 50 °C and 60 °C which is in line with other investigators.

In the earlier paper [4] we already reported on the reproducibility after various events in some detail. These events included venting, bake-out, exposure to "active" gases O_2, CO and CO_2, drop-down tests and transport. For all these events, the sensitivity changed by less than 1 %.

Table 2
Change in sensitivity for He, N_2 and Ar after the conditioning procedure at Ar pressure 5 mPa and electron emission 30 μA (relative to the value before each conditioning). The conditioning time was varied and is given in the second column. Gauge X004 was conditioned in two different laboratories, IMT and PTB with transport and venting in between. For gauge X010, after the 4th conditioning the gauge was exposed to atmosphere (vented) and after this baked out at 150 °C, 48 h.

	time in h	Gas			Gauge
		He	N_2	Ar	
After 1st conditioning	1	−10.1 %	−2.1 %	−0.47 %	X005
After 1st conditioning	1	−9.0 %	−1.9 %	−0.59 %	X004
After 2nd conditioning	1	−2.8 %	−0.54 %	−0.39 %	at PTB
After 1st conditioning	1.6	−8.7 %	/	−0.7 %	X004
After 2nd conditioning	3	−2.0 %	−1%	−0.7 %	at IMT
After 3rd conditioning	3	−0.6 %	−0.3 %	−0.2 %	
After 1st conditioning	1	/	−0.5 %	−0.2 %	X010
After 2nd conditioning	1	/	−0.3 %	−0.2 %	
After 3rd conditioning	2	/	−0.5 %	−0.4 %	
After 4th conditioning	2		−0.4 %	−0.5 %	
Venting + baking					
After 1st conditioning	2	/	−1.0 %	−0.3 %	
After 2nd conditioning	2	/	−0.1 %	0.4 %	

An example for repeatability is shown in Fig. 5. A calibration pressure of 1×10^{-5} Pa was generated 10 times in a period of approximately-one hour. Between pressure points the system was evacuated to the base pressure below 1.5×10^{-7} Pa. The relative difference between maximum and minimum value of sensitivity was 0.06 %. Relative standard deviation of 10 measured values is 0.019 %. This result shows an excellent repeatability.

If the sensitivity of an ionisation vacuum gauge (IG) is known for each gas species in a mixture and if there are no interference effects, the gauge can be used to calibrate a quadrupole mass spectrometer (QMS) for a mixture. To this end, gas A can be admitted into a system where IG and QMS are mounted on equivalent positions with equal pressure. By the known sensitivity for gas A of IG, the pressure p_A can be determined from the collector current I_A and the QMS calibrated for gas A. Then, another gas B is introduced, and the IG will indicate the current $I_A + I_B$. When knowing the sensitivity for gas B, partial pressure p_B can be determined from the collector current I_B and the QMS calibrated for the gas mixture A and B. This can be continued with other gases.

It is necessary that the presence of gas B does not change the sensitivity for gas A in the IG. Often, this is not the case for a QMS because of its complex structure, but we can expect that this is true for the gauge of the new design, since there are no significant space charge effects.

We tested this claim by adding known pressures of nitrogen gas to an argon pressure of $3{\cdot}10^{-5}$ Pa. By measuring the additional ion currents and applying the respective sensitivities, the calculated total pressure of the IG agreed within 0.5 % to the sum of the known pressures of nitrogen and argon. No significant interference effect was visible.

The resolution limit is mainly determined by the resolution of the current meter measuring the ion current and the stability of the residual offset current. A resolution of $3{\cdot}10^{-14}$ A was demonstrated at a measured residual offset current of 1 pA. With an emission current of 33 μA and the nominal sensitivity for nitrogen 0.29 Pa^{-1}, the resolution pressure limit is $3{\cdot}10^{-9}$ Pa. The residual offset current of 1 pA corresponds to a pressure of $1{\cdot}10^{-7}$ Pa and is the sum of two contributions: residual pressure of the calibration system itself and outgassing of the gauge in operation.

Another measurement of the gauge resolution is shown in Fig. 6, where the response of an extractor gauge and the new gauge to a very small value of generated N_2 calibration pressure was measured at the same time in the same system. The extractor gauge indicated a change in pressure reading near 2900 s of $1.92{\bullet}10^{-9}$ Pa to the base level of $1.455{\bullet}10^{-7}$ Pa. At the same time the recorded change of the collector current was 0.0174 pA to the base level of 1.63 pA. At nominal sensitivity 0.29 Pa^{-1} and an emission current of 31 μA the indicated change of N_2 pressure by the gauge is $1.94{\bullet}10^{-9}$ Pa, the base level is $1.81{\bullet}10^{-7}$ Pa. To reduce noise of the ion current measurement at these low levels, the readings of the picoammeter were averaged over a time interval of 15 s.

Fig. 7 shows the linearity of the ion current with electron emission current up to 300 μA, at two different values of Ar pressure: $1{\bullet}10^{-4}$ Pa and $1{\bullet}10^{-3}$ Pa. These measurements show that even at emission currents that are almost 10 times higher than the nominal emission current for the gauge (30 μA) there is no space charge influence, which was also confirmed for $1{\bullet}10^{-2}$ Pa. The slightly different slopes at the two pressures in Fig. 7 stem from a non-linearity of the reference gauge. For our conclusion, the linear slope with emission current is important, only. Non-linearities beyond $1{\bullet}10^{-2}$ Pa can be reduced by reducing the electron current.

5. Influence of magnetic fields

Earth's magnetic fields (25–65 μT) can influence the trajectories of 200 eV electrons. While the magnetic field has little effect on Bayard-Alpert type gauges [8], because a swarm of electrons with many directions is emitted from the filament, this should not be the case with the ISO gauge, where all electrons point into the same direction. Indeed, simulations showed that T_e drops to 0 with a gauge in uniform magnetic

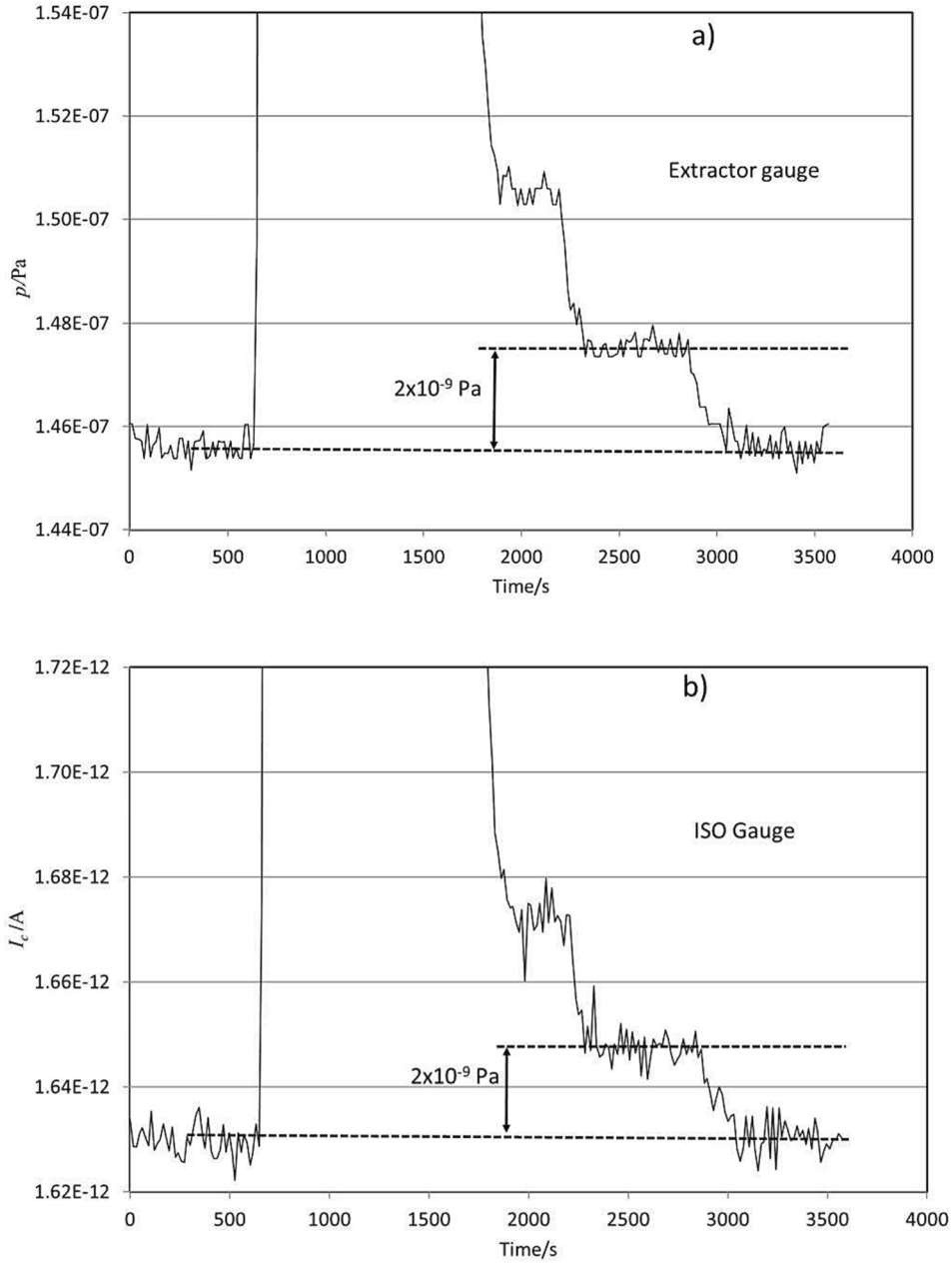

Fig. 6. Comparison of pressure reading of extractor gauge (a) to the ion collector reading for novel gauge (b) to pressure reading during a stepwise reduction of the pressure of nitrogen. Both gauges detect the pressure step of $2 \bullet 10^{-9}$ Pa near 2900s.

field of 200 μT along x-axis [3]. Here we add more simulation results and an experimental study of the influence of the magnetic field on the operation of the ISO gauge.

Simulations have been performed with charged particle optics software SIMION, using the approaches described in detail in [9] and under the assumption of a constant magnetic field along the electron beam. The simulations enabled to evaluate the magnetic field influence on the primary electron trajectories, the electron path length within the ionisation cage, and the gauge sensitivity.

Simulations showed that the relative change of the electron path length due to a magnetic field in the z-direction of up to 1 mT can be safely neglected. Fig. 8 shows the measured relative change in sensitivity with an axial magnetic field produced by a solenoid on a vertically installed gauge not in line with the Earth's magnetic field. Within the range of ± 1 mT (±0.4 A) the changes lie well within the (statistical) measurement uncertainties and within ± 2.5 mT (±1 A) still within 1 %.

For an electron beam not perfectly aligned with the z-axis, it can be expected that the electron path and hence the sensitivity will be increased. This effect will be amplified with higher magnetic flux density. The trend of increasing sensitivity with the magnetic flux density due to the longer electron path can be observed at the two ends of the graph.

Along the x- and y-axis we performed simulations of the deflection of the electron beam with magnetic fields. The electron beam deflection along the x-axis in the circular exit region of the anode cage induced by a magnetic field component B_y is linear with a deflection constant $\Delta x/\Delta B_y = 0.04987$ mm/μT. Deflection along the y-axis (caused by the magnetic field component B_x) is somewhat non-linear, most probably due to its superposition with the deflection by the electric field of the collector rod. The deflection vs magnetic field can be described by a parabolic dependence $\Delta y = 0.04079 \bullet B_x + 1.62 \bullet 10^{-5} \bullet B_x^2$.

We also performed experimental studies of the deflection of the

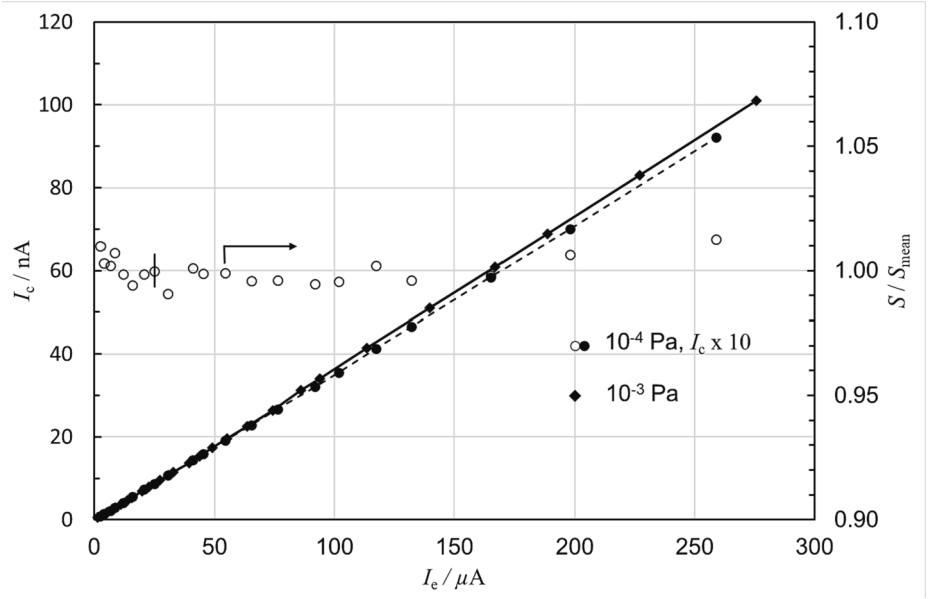

Fig. 7. Ion collector current vs electron emission current at two different argon pressures (left scale, filled symbols). Open symbols, right scale indicate the linearity by the variation of sensitivity divided by the mean sensitivity.

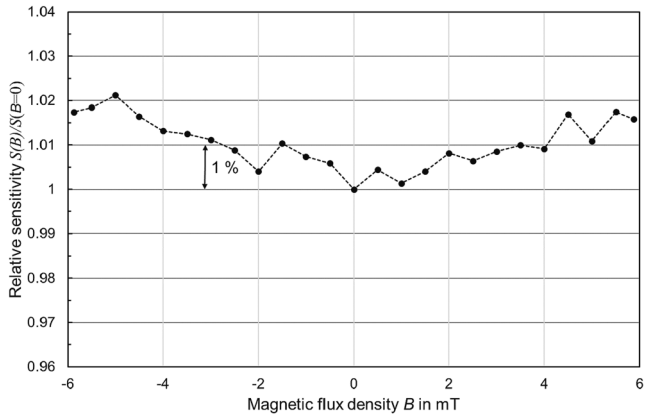

Fig. 8. Relative change of sensitivity with axial magnetic flux density generated with a solenoid of 2.5 mT/A. Faraday at 280 V, Wehnelt at 34 V, pressure at 9•10^{-4} Pa argon.

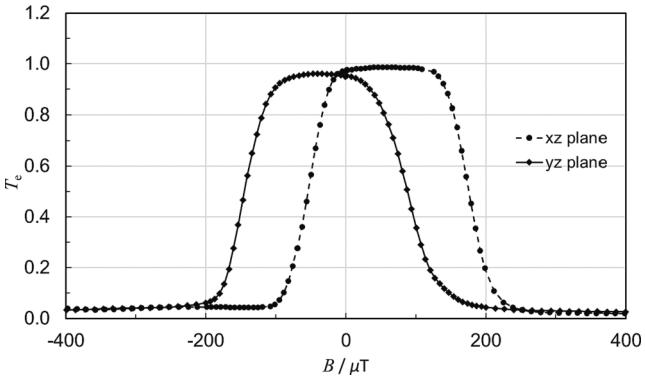

Fig. 9. Electron transmission efficiency T_e as a function of the deflecting magnetic field flux in xz and yz planes (see Fig. 1).

electron beam with magnetic fields perpendicular to the z-axis by mounting home-made Helmholtz coils with a diameter of about 850 mm, coil constant 0.664 mT/A, providing a uniformity of 2 μT at 1 mT, within 10 vol%. The gauge was oriented along the Earth's magnetic field, securing its negligible influence on the gauge operation as it will be demonstrated below.

Fig. 9 shows the measured electron transmission efficiency vs the magnetic flux density B. Electron current was about 33 μA and the Wehnelt potential 34 V. The existence of the T_e plateaus indicates that the electron beam diameter is smaller than the circular anode exit tube diameter of 10 mm. Full width at half maximum of the two dependences should approximately correspond to the deflection of beams over the diameter of the circular exit, being 228 and 230.5 μT along the x and y axes, respectively. These results fit quite well with the corresponding simulation predictions of 200.5 and 246 μT. The width of the plateaus in Fig. 9 suggests that external magnetic field in the plane normal to the gauge axis should not exceed 30–50 μT in the case of perfectly aligned gauges, which is why magnetic shielding (e.g. using μ-metal) is recommended.

In Fig. 10 the damping of the Earth's magnetic field applied perpendicular to the symmetry axis is shown as a function of position within a CF63 nipple with the tubular section made from μ-metal (the gauge position is shown for illustration). In the centre, the magnetic flux density is only 1.2 % of the applied flux density.

By means of the plateau slopes (Fig. 9) it is also possible to estimate the diameter of the electron beam near the cage exit. Assuming a cylinder symmetric electron beam, the width at 50 % of T_e indicates the position where the beam centre hits the edge of the exit tube. With a linear dependence of electron beam deflection with the magnetic flux, which was confirmed by the simulation, the first derivative of the curve in Fig. 9 indicates an electron beam diameter of 2.9 mm FWHM. The diameter at 10 % is about 5.9 mm.

Varying the Wehnelt potential and the emission current we found that the beam size slightly broadens with increasing Wehnelt potential and emission current. We also experimentally found that the Wehnelt potential may cause a shift of the electron beam centre from the anode exit tube axis in some cases, probably due to a small misalignment of the emitter.

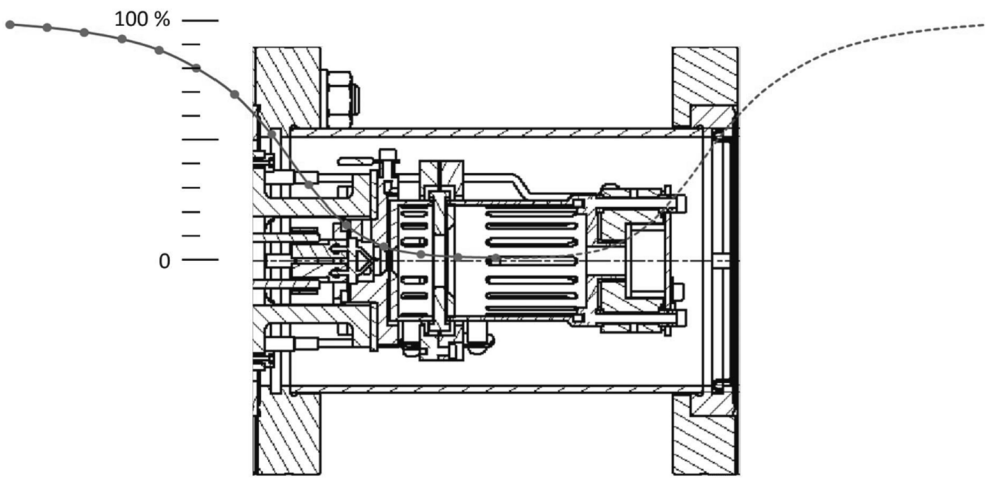

Fig. 10. Damping of a magnetic flux density applied perpendicular to the axis of the ionisation gauge by means of a CF63 nipple with the tubular section made from μ-metal.

Table 3
Mean relative gas sensitivity factors S_X/S_{N2} determined for the new ionisation vacuum gauge design. These factors were determined between 10^{-4} Pa and 10^{-2} Pa. The variation between different gauges is expressed in the 3rd column as standard deviation. The number of tested gauges varied between 2 and 10 (except for H_2O) and was typically 3. Columns 5 to 7 show the ratios of the ionisation cross sections σ_X/σ_{N2} at the energies or positions specified. It should be noted that in contrast to the experimental values in column 2, the values in column 5 to 7 do solely consider the ratios of ionisation cross sections, but not secondary effects as secondary electrons by ion impact, fragmentation of molecules, ion collection efficiency and others.

Gas species	S_X/S_{N2}	St.dev.	S_X/S_{N2} (sim.)	σ_X/σ_{N2} @200 eV	σ_X/σ_{N2}@75 eV	σ_X/σ_{N2}@peak
H_2	0.374	0.0151	0.350	0.323 [11]	0.38 ± 0.04 [14]	0.384 [15]
He	0.176	0.0049	0.145	0.144 [11]	0.132 [11]	0.138 [11]
				0.152 [12]	0.131 [12]	0.143 [12]
				0.139 [13]	0.120 [13]	0.133 [13]
					0.13 ± 0.02 [14]	0.148 [15]
CH_4	1.386	0.013	1.25	1.18 [11]	1.384 [11]	1.348 [11]
					1.63 ± 0.30 [14]	1.46 [15]
Ne	0.337	0.015	0.300	0.344 [12]	0.215 [12]	0.299 [12]
				0.318 [13]	0.199 [13]	0.277 [13]
H_2O	0.832		0.899	0.891 [11]	0.905 [11]	0.899 [11]
N2	1.000		1.000	1.000	1.000	1.000
CO	1.021	0.0030	1.009	1.00 [11]	1.00 [11]	1.00 [11]
O_2	0.964	0.057	1.024	1.05 [11]	0.979 [11]	0.979 [11]
CO_2	1.433	0.029	1.468	1.47 [11]	1.41 [11]	1.43 [11]
Ar	1.134	0.013	1.11	1.053 [12]	1.105 [12]	1.093 [12]
				1.048 [13]	1.100 [13]	1.108 [13]
					1.23 ± 0.07 [14]	1.13 [15]
Kr	1.523	0.0062	1.572	1.521 [12]	1.668 [12]	1.628 [12]
				1.414 [13]	1.574 [13]	1.540 [13]
Xe	2.193	0.067	2.22	2.260 [12]	2.016 [12]	2.089 [12]
				2.129 [13]	2.141 [13]	2.204 [13]
					2.62 ± 0.08 [14]	2.16 [15]

6. Relative sensitivity factors and ionisation probability

Table 3 lists the relative gas sensitivity factors as defined in ISO 27894 [10] for several species. Columns 2 and 3 show the experimental mean values and their standard deviation for different gauges. The variations between the gauges are very small, which is a great success of this new design. Column 4 shows the relative gas sensitivity factors as obtained from simulations which consider the actual kinetic energy of the electrons on their path through the ionisation volume. Column 5 gives the ratio of the ionisation cross sections of electrons at 200 eV, which is due to the variation of electron energy inside the ionisation volume only an estimate for the relative gas sensitivity factor. For this reason, columns 6 and 7 give the ratios at 75 eV or near the peak maximum, which position varies from gas to gas between 80 eV and 180 eV. The values have been taken from refs. [11] as indicated in the table. The standard uncertainties of the values were estimated to 10 % in [11], to 7 % in [12] and 5 % in [13], for [14] they are given in the table. Considering these uncertainties and the variations between investigators affecting also the simulation results, the agreement between the measured relative sensitivity factors and ratios obtained from ion cross sections and simulations seems fair, except for helium. The experimental data base for the new gauge, however, needs to be extended to come to sharper conclusions.

It should be noted here that in Bayard-Alpert gauges the mean electron energy inside the ionisation space varies from gauge to gauge, depends on pressure and time so that the ionisation probability is changing as well as the relative gas sensitivity factor [16–28]. In our gauge design, however, the electron energy inside the ionisation space does not depend on the individual gauge or pressure and is stable.

7. Discussion and summary

Additional simulations and measurements were performed to characterise the new ionisation vacuum gauge type, mainly to enable the development of an ISO Technical Specification (ISO TS 6737). This ISO TS 6737 shall enable any experienced manufacturer of vacuum gauges or vacuum components to produce this ionization vacuum gauge.

Compared to the original design parameters for the potentials we found more suitable values for the Wehnelt and Faraday potentials, which will be recommended in the TS 6737. It was also found that a variation of 0.5 % about the recommended values for all potentials has no significant influence on the performance and parameters of the gauge. Simulations indicated that some geometrical modifications may not be critical for the parameters like sensitivity, electron transmission efficiency and ion collection efficiency, but, since these have not been tested experimentally yet, it is recommended not to consider them in the ISO TS 6737.

Measurements of the influence of the magnetic flux have shown that a magnetic flux perpendicular to the direction of the electron beam within the anode cage greater than 50 μT may alter the electron beam in a significant manner so that the parameters of the gauge are changed. This value is close to the flux of the earth magnetic field so that a magnetic shield is recommended.

A follower of the European project which developed the new gauge, the project EMPIR 20SIP01, is collaborating with the ISO TC 112 Vacuum technology to develop ISO TS 6737. Publication is expected for 2023.

CRediT authorship contribution statement

Karl Jousten: Conceptualization, Methodology, Validation, Formal analysis, Resources, Data curation, Visualization, Supervision, Project administration, Funding acquisition. **Sylke Bechstein:** Investigation, Validation, Visualization. **Matthias Bernien:** Methodology, Validation, Formal analysis. **Frédéric Boineau:** Validation, Formal analysis, Investigation. **Nenad Bundaleski:** Conceptualization, Methodology, Validation, Formal analysis, Investigation, Resources, Data curation, Writing – review & editing, Visualization. **Claus Illgen:** Formal analysis, Investigation. **Berthold Jenninger:** Methodology, Validation, Formal analysis, Investigation, Resources, Data curation, Writing – review & editing, Visualization. **Janez Šetina:** Methodology, Validation, Formal analysis, Investigation, Writing – review & editing, Visualization. **Ricardo A.S. Silva:** Validation, Formal analysis, Investigation. **Anke Stöltzel:** Validation, Formal analysis, Investigation. **Orlando M.N.D. Teodoro:** Methodology, Resources, Writing – review & editing, Supervision, Project administration, Funding acquisition. **Martin Wüest:** Methodology, Validation, Resources, Visualization, Funding acquisition.

Declaration of Competing Interest

The authors declare the following financial interests/personal relationships which may be considered as potential competing interests: Karl Jousten reports financial support was provided by Physikalisch-Technische Bundesanstalt. Ricardo Silva reports financial support was provided by Nova University of Lisbon.

Data availability

Data will be made available on request.

Acknowledgements

This work has received funding from the EMPIR programme (projects 16NRM05 and 20SIP01) co-financed by the Participating States and from the European Union's Horizon 2020 research and innovation programme and the Portuguese National Funding Agency for Science, Research and Technology in the framework of the project UIDB/FIS/ 00068/2020.

References

[1] K. Jousten, F. Boineau, N. Bundaleski, C. Illgen, J. Setina, O.M.N.D. Teodoro, M. Vicar, M. Wüest, A review on hot cathode ionisation gauges with focus on a suitable design for measurement accuracy and stability, Vacuum 179 (2020), 109545, https://doi.org/10.1016/j.vacuum.2020.109545.
[2] A. Klopfer, An ionization gauge for measurement of Ultra-high vacua, Transact. of the 8th Nat. Symp. of the AVS and 2nd Int. Congr., Pergamon, New York, 1962, 439.
[3] B. Jenninger et al., Development of a design for an ionisation vacuum gauge suitable as a reference standard, Vacuum 2020,109884, https://doi: 10.1016/j.vacuum.2020.109884.
[4] K. Jousten, et al., Electrons on a straight path: A novel ionisation vacuum gauge suitable as reference standard, Vacuum 189 110239 (2021), https://doi.org/10.1016/j.vacuum.2021.110239 and arXiv:2103.03566.
[5] https://en.wikipedia.org/wiki/Wehnelt_cylinder.
[6] N. Bundaleski, et al., Novel ionisation vacuum gauge suitable as a reference standard: influence of primary electron trajectories on the operation, Vacuum 201 (2022), 111041, https://doi.org/10.1016/j.vacuum.2022.111041.
[7] I. Figueiredo, et al., Influence of ion induced secondary electron emission on the stability of ionisation vacuum gauges, Vacuum 184 (2021), 109907, https://doi.org/10.1016/j.vacuum.2020.109907.
[8] R.A.S. Silva, N. Bundaleski, O.M.N.D. Teodoro, Effect of the magnetic field on the operation of ionisation gauges, Vacuum 204 (2022), 111339, https://doi.org/10.1016/j.vacuum.2022.111339.
[9] R. Silva, N. Bundaleski, A.L. Fonseca, O.M.N.D. Teodoro, 3D-Simulation of a Bayard-Alpert ionisation gauge using SIMION program, Vacuum 164 (2019) 300.
[10] ISO 27894:2009 Vacuum technology — Vacuum gauges — Specifications for hot cathode ionization gauges.
[11] Database published by NIST (received on 2022-08-16), for molecules: https://physics.nist.gov/PhysRefData/Ionization/molTable.html, for atoms: https://physics.nist.gov/PhysRefData/Ionization/atom_index.html. This data base includes values from ref. [12].
[12] D. Rapp, P. Englander-Golden, Total Cross Sections for Ionization and Attachment in Gases by Electron Impact. I. Positive Ionization, J. Chem. Phys. 43, 1464-1479 (1965); https://doi.org/10.1063/1.1696957.
[13] R. Rejoub, B.G. Lindsay, R.F. Stebbings, Determination of the absolute partial and total cross sections for electron-impact ionization of the rare gases, Phys. Rev. A 65 (2002), 042713.
[14] F. Nakao, Determination of the ionization gauge sensitivity using the relative ionization cross-section, Vacuum 25 (1975) 431–435, https://doi.org/10.1016/0042-207X(75)90491-1.
[15] Summers R.L., NASA Technical Note TN D-5285, Washington DC, June 1969.
[16] P.J. Abbott, J.P. Looney, Influence of the filement potential wave form on the sensitivity of glass-envelope Bayard-Alpert gages, J. Vac. Sci. Technol. A 12 (5) (1994) 2911–2916.
[17] P.C. Arnold, D.G. Bills, Causes of unstable and nonreproducible sensitivities in Bayard-Alpert ionization gauges, J. Vac. Sci. Technol. A 2 (2) (1984) 159–162.
[18] P.C. Arnold, S.C. Borichevsky, Nonstable behavior of widely used ionization gauges, J. Vac. Sci. Technol. A 12 (2) (1994) 568–573.
[19] H.U. Becker, G. Messer, Sensitivity dependence on collector surface properties in ion gauges, Vide Suppl. 201 (1980) 234–237.
[20] H.U. Becker, G. Messer, The influence of ion collector and electrode surface properties as well as geometrical arrangement on variations of ionization gauge coefficients, Proc. IX IVC-V ICSS, Madrid (1983), Ext. Abstract, 84.
[21] D.G. Bills, Causes of nonstability and nonreproducibility in widely used Bayard-Alpert ionisation gauges, J. Vac. Sci. Technol. A 12 (2) (1994) 574–579.
[22] G. Comsa, Ion Collection in Bayard-Alpert Gauges, J. Vac. Sci. Technol. 9 (1) (1972) 117–121.
[23] J.A. Fedchak, D.R. Defibaugh, Long-term stability of metal-envelope enclosed Bayard-Alpert ionization gauges, J. Vac. Sci. Technol. A 30 (6) (2012), 061601.
[24] C.P. Gopalaraman, R.A. Armstrong, P.A. Redhead, Sensitivity variations in Bayard-Alpert gauges caused by Auger emission at the collector, J. Vac. Sci. Technol. 7 (1) (1970) 195–198.
[25] J. Groszkowski, Unreliability of ionization gauges and its consequences, Bull. Acad. Polon. Sci 9 (4) (1961) 235–237.
[26] K. Jousten, P. Röhl, Instability of the spatial electron current distribution in hot cathode ionization gauges as sources of sensitivity changes, J. Vac. Sci. Technol. A 13 (4) (1995) 2266–2270.
[27] R.N. Peacock, N.T. Peacock, Sensitivity variation of Bayard-Alpert gauges with and without closed grids from 10^{-4} to 1 Pa, J. Vac. Sci. Technol. A 8 (4) (1990) 3341–3344.
[28] C.R. Tilford, A.R. Filippelli, P.J. Abbott, Comments on the stability of Bayard-Alpert ionization gages, J. Vac. Sci. Technol. A 13 (2) (1995) 485–487.